



New Virtual Test Bed Capabilities: Virtual DOME Model and New Updates to Repository

August 2024

Fiscal Year 2024 Activities Overview

Lise Charlot, Mustafa Jaradat, Mohamed Elkamash, Guillaume Guidicelli, Abdalla Abou Jaoudé

Idaho National Laboratory

Emily Shemon, Shikhar Kumar, Joffrey Dorville

Argonne National Laboratory





DISCLAIMER

This information was prepared as an account of work sponsored by an agency of the U.S. Government. Neither the U.S. Government nor any agency thereof, nor any of their employees, makes any warranty, expressed or implied, or assumes any legal liability or responsibility for the accuracy, completeness, or usefulness, of any information, apparatus, product, or process disclosed, or represents that its use would not infringe privately owned rights. References herein to any specific commercial product, process, or service by trade name, trade mark, manufacturer, or otherwise, does not necessarily constitute or imply its endorsement, recommendation, or favoring by the U.S. Government or any agency thereof. The views and opinions of authors expressed herein do not necessarily state or reflect those of the U.S. Government or any agency thereof.

REVISION LOG

Revision No.	Date	Affected Pages	Description
0	08/31/24	All	New document.

SUMMARY

The Department of Energy (DOE) Office of Nuclear Energy National Reactor Innovation Center accelerates the deployment of novel reactor concepts by establishing both physical and virtual spaces for building and testing various components, systems, and complete pilot plants. The Virtual Test Bed represents the virtual arm of the National Reactor Innovation Center and is a joint effort with the DOE Nuclear Energy Advanced Modeling and Simulation Program.

The Virtual Test Bed mission is to accelerate the deployment of advanced reactors by facilitating the adoption of cutting-edge DOE advanced modeling and simulation tools to design, evaluate, and license reactors. This is primarily achieved by storing example challenge problems in an externally available repository and by developing models to fill the M&S gaps needed for potential demonstrators.

Activities conducted this fiscal year focused on developing of a Demonstration of Microreactor Experiments shield model to help accelerate the confirmatory analysis required for the reactor demonstration. This model and workflow will allow developers to leverage advanced modeling and simulation tools to ensure their reactor demonstration concept will meet dose requirements and that the surrounding shield will stay within concrete temperature limits during steady-state and transient operation conditions. An initial model has been developed to evaluate the temperature distribution in the concrete shield during steady-state operation, including neutron and gamma heating effects. Various modeling strategies have been examined to understand their applicability and limitations with different reactor designs to make the workflow as reactor-agnostic as possible and computationally effective to maximize its usability.

In addition to describing the Demonstration of Microreactor Experiments shield model and associated results, this report summarizes other accomplishments regarding repository maintenance and improvement and new external models hosted on the repository.

ACKNOWLEDGEMENTS

This document was sponsored by the National Reactor Innovation Center (NRIC). NRIC is a national program funded by U.S. Department of Energy's Office of Nuclear Energy and is dedicated to the demonstration and deployment of advanced nuclear energy. Neither the U.S. Government nor any agency thereof makes any warranty, express or implied, or assumes any legal liability or responsibility for the accuracy, completeness, or usefulness of any information, apparatus, product, or process disclosed, or represents that its use would not infringe on privately owned rights. References herein to any specific commercial product, process, or service by trade name, trademark, manufacturer, or otherwise do not necessarily constitute or imply its endorsement, recommendation, or favoring by the U.S. Government or any agency thereof. The views and opinions of authors expressed herein do not necessarily state or reflect those of the U.S. Government or any agency thereof.

CONTENTS

1.	Introduction.....	8
2.	Initial DOME Shield Virtual Model	9
2.1	OpenMC Reactor Physics Model.....	12
2.1.1	Reference One-Step Approach.....	12
2.1.2	Generic Two-Step Approach.....	13
2.1.3	Enhanced Step 2 Approach: <i>Enhancing Particle Transport Inside the Cavity in Step 2</i>	15
2.1.4	Enhanced Step 1 Approach: <i>Accounting for Reactivity Feedback in Step 1</i>	17
2.1.5	Comparison of approaches for simplified geometry	18
2.1.6	Recommendations on Selecting of a Two-Step Approach.....	21
2.1.7	OpenMC Models of the DOME Microreactor and Shield using the Generic Two-Step Approach.....	22
2.1.8	Comparison of approaches for DOME shield model	26
2.2	MOOSE Thermal Model.....	27
2.2.1	Base Thermal Model Results	30
2.2.2	Comparison with the ANSYS Model	31
2.2.3	Sensitivity Analysis.....	32
2.3	Cardinal Model	34
2.3.1	Coupled Cardinal Simulation Results Using the Generic Two-Step approach.....	34
2.3.2	Comparison of Approaches for Cardinal model of DOME Shield Model	36
2.4	Future Work.....	37
3.	Repository Updates.....	39
3.1	New Models Ported in FY24	39
3.2	Workflow improvements	40
3.2.1	Creation of Templates for Contributions on GitHub.....	40
3.2.2	High-Performance Computing Integration	40
3.2.3	Trainings and Workshop Sessions	41
3.3	Website Improvements.....	41
3.4	Repository Maintenance.....	42
4.	Conclusion.....	43
5.	References	44

FIGURES

Figure 2-1. The DOME test bed and supplemental shield structure.....	9
Figure 2-2. Supplemental shield structure with the microreactor experiment shown in green (FY23 conceptual design [2]).	10
Figure 2-3. Proposed multistep computational workflow of DOME shield neutronics and thermal calculations under MOOSE framework.	11
Figure 2-4. Reference one-step approach.....	13
Figure 2-5. Generic two-step approach.	14
Figure 2-6. Enhanced Step 2 approach.....	16
Figure 2-7. Enhanced Step 1 approach.....	17
Figure 2-8. Simplified OpenMC model.....	18
Figure 2-9. Difference in keff between the reference and two-step approach variations for different backscattering current ratios.....	20
Figure 2-10. Relative difference in heat deposited in the shield between the reference and two-step approach variations for different backscattering current ratios.	21
Figure 2-11. Cross-sectional view of microreactor OpenMC model (x-z slice).	23
Figure 2-12. Axial view of combined reactor and shield OpenMC models.....	24
Figure 2-13. Neutron and gamma fluxes compared to the specification.	24
Figure 2-14. Neutron and gamma fluxes for the eigenvalue problem.	25
Figure 2-15. Neutron and gamma fluxes and heat rate in the DOME shield for the fixed source problem.	25
Figure 2-16. Computational mesh used for the heat transfer model.	28
Figure 2-17. Mesh details of the insulation layers covering the floor, doors and ceiling.	28
Figure 2-18. Thermal model geometry including the reactor box.	29
Figure 2-19. Temperature distribution in the concrete for the thermal base model.	31
Figure 2-20. Comparison of the MOOSE and ANSYS thermal models.	32
Figure 2-22. Sensitivity analysis of the maximum concrete temperature with respect to the cavity thermal conductivity.	33
Figure 2-23. Sensitivity analysis of the maximum concrete temperature with respect to the reactor surface emissivity.	33
Figure 2-24. Power density in the DOME shield due to neutron and gamma heating.	35

Figure 2-25. Temperature in the DOME shield due to neutron and gamma heating.	35
Figure 3-1. Pull request template, reminding the potential contributor that an EC step must be performed before contributing.	41
Figure 3-2. Screenshots from the additional developments of the filtering capability.	42
Figure A-1. Trajectory of a particle entering a shield twice.	46

TABLES

Table 1. Summary of investigated approaches	18
Table 2. Heat source distribution within the shield.	26
Table 3. Comparison of heat source in the shielding region comparing various OpenMC one- and two-step modeling approaches.	26
Table 4. Material properties used in the thermal model	30
Table 5. Comparison of peak concrete temperature in shielding region comparing various OpenMC one- and two-step modeling approaches.	36
Table 6. Models uploaded to the VTB repository in FY24.	39
Table 7. Repository maintenance in FY24.	42
Table 8. Heat H_{ES1} deposited in the shield for different outcomes using the ES1 approach	47

ACRONYMS

DOE	U.S. Department of Energy
DOME	Demonstration of Microreactor Experiments
ES1	Enhanced Step 1
ES2	Enhanced Step 2
FHR	Fluoride-Salt-Cooled High-Temperature Reactor
FY	Fiscal Year
G2S	Generic two-step
HTGR	High Temperature Gas Reactor
INL	Idaho National Laboratory
LFR	Lead Fast Reactor
MOOSE	Multiphysics Object-Oriented Simulation Environment
M&S	Modeling and Simulation
MSR	Molten-Salt Reactor
NNSA	National Nuclear Security Administration
NEAMS	Nuclear Energy Advanced Modeling and Simulation
NRIC	National Reactor Innovation Center
R1S	Reference one step
SFR	Sodium Fast Reactor
VTB	Virtual Test Bed

New Virtual Test Bed Capabilities: Virtual DOME Model and New Updates to Repository

1. INTRODUCTION

The Department of Energy (DOE) Office of Nuclear Energy National Reactor Innovation Center (NRIC) accelerates the deployment of novel reactor concepts by establishing both physical and virtual spaces for building and testing various components, systems, and complete pilot plants. The Virtual Test Bed (VTB) represents NRIC's virtual arm and is a joint effort with the DOE Nuclear Energy Advanced Modeling and Simulation (NEAMS) Program.

The VTB mission is to accelerate the deployment of advanced reactors by facilitating the adoption of cutting-edge DOE advanced modeling and simulation (M&S) tools to design, evaluate, and license reactors. This is primarily achieved by storing example challenge problems in an externally available repository and by developing models to fill the M&S gaps needed by potential demonstrators.

Activities conducted this fiscal year (FY) focused on developing of a Demonstration of Microreactor Experiments (DOME) shield model to accelerate the confirmatory analysis required for the reactor demonstration. This model and workflow will allow developers to leverage advanced M&S tools to ensure their reactor demonstration concept will meet dose requirements and the surrounding shield will stay within concrete temperature limits during steady state and transient operation conditions. An initial model has been developed to evaluate the temperature distribution in the concrete shield during steady-state operation, including neutron and gamma heating effects. Various modeling strategies have been examined to understand their applicability and limitations with different reactor designs to make the workflow as reactor-agnostic as possible as well as computationally effective to maximize its usability.

In addition to describing of the DOME shield model and associated results, this report summarizes other accomplishments regarding repository maintenance and improvement and new external models hosted on the repository.

2. INITIAL DOME SHIELD VIRTUAL MODEL

The Experimental Breeder Reactor-II dome containment structure is being refurbished to host advanced reactor demonstrations, specifically microreactor experiments. The refurbished facility is known as DOME. The facility will provide safety-class confinement supporting the operation of nuclear reactors. A supplemental shielding system is needed to meet dose rate and activation limits at the Idaho National Laboratory (INL) Materials and Fuels Complex [1]. The shield layout within the DOME test bed is shown in Figure 2-1.

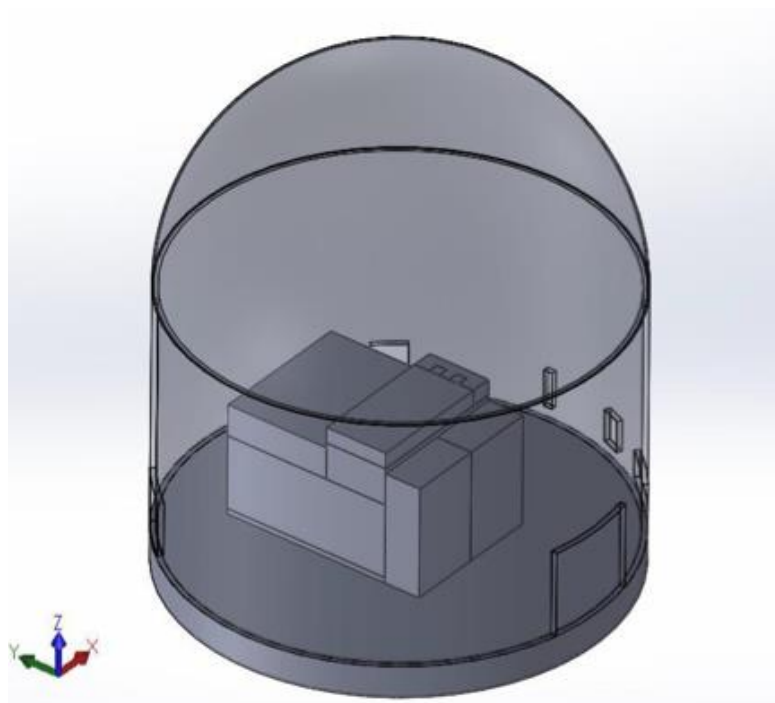


Figure 2-1. The DOME test bed and supplemental shield structure.

The shield design has not been finalized at the issue time of this report, and consequently, this analysis uses a conceptual design to establish a methodology to predict how a microreactor concept at full power will influence the temperature of the concrete shield. The supplemental shield design is taken from Reference [2] and shown in Figure 2-2. It includes a U-shaped tank, shown in blue, that circulates water to maintain a maximum outlet temperature of about 300 K (80°F). Two sliding door pieces made with magnetite high-density concrete allow access to the inside of the shield through the front. The roof, walls, shield floor, and doors are primarily made of high-density magnetite concrete but have an internal layer of ordinary concrete covered with four 0.25-inch-thick layers of insulation, alternating between aluminum and RESCOR-60 materials.

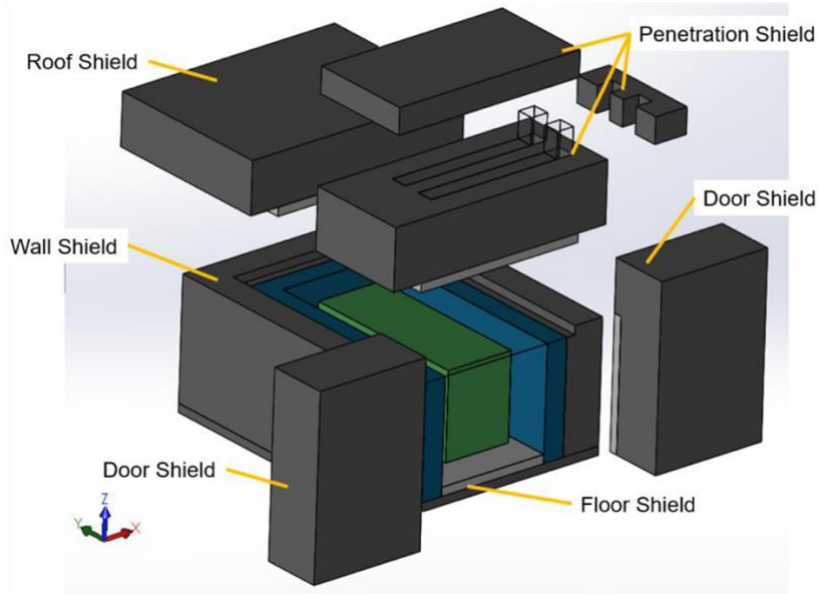


Figure 2-2. Supplemental shield structure with the microreactor experiment shown in green (FY23 conceptual design [2]).

The following requirements were formulated to maximize model usability:

- The shield model should leverage open-source codes, to the extent possible, to facilitate code access and adoption
- The shield model should couple to the reactor in a manner that is as agnostic to the reactor design as possible, since multiple vendor concepts will be housed within the shield at different points in time
- The model should be easily modifiable to accommodate shield configuration changes
- The model and workflow should minimize computational cost while maintaining high accuracy

Keeping the *open-source* code preference in mind, Cardinal was selected for this model. Cardinal [3] is an open-source application that couples the Monte Carlo reactor physics code OpenMC [4] and computational fluid dynamics code NekRS to the MOOSE (Multiphysics Object-Oriented Simulation Environment) framework and physics modules [5], allowing for efficient data transfer between physics applications. Note that the DOME shield model uses only the OpenMC (reactor physics) and MOOSE (heat transfer) capabilities.

Keeping the *remaining three requirements* in mind, a modeling workflow was conceived where the core and shield are modeled separately and linked through boundary conditions. Because the reactor physics calculations are performed in two geometrically-isolated steps (Step 1 and 2), this method is referred to as the two-step method. This multistep nature simplifies the user burden considerably as the user can create a detailed core model without detailed knowledge of the core shield other than inner cavity dimensions. The user can then leverage the reactor physics and thermal

fluids shield models developed in this work almost immediately. This is expected to help streamline future confirmatory analyses. Users of the DOME reactors are expected to have already completed step 1 of the process independently as part of their design process. In the future, step 2 could be automated (e.g., via digital engineering tools) in order to directly import a vendor-generated model in (with the capabilities in step 1) to rapidly proceed through the rest of the work flow (step 2) and estimate important safety bounds for testing within DOME. In this initial report however, the workflow for the various steps is established and automation of the process is left for future work.

The two-step neutronics approach provides maximum flexibility to users but introduces approximations which may impact accuracy. The proposed workflow is shown in Figure 2-3, and is evaluated in detail in this report (as well as variations of it):

1. The detailed microreactor is modeled inside of the shield cavity surface. Vacuum boundary conditions are imposed at the interior shield cavity surface to represent no re-entrant particles from outside the core. An OpenMC reactor physics eigenvalue problem is performed to tally the surface source on the interior shield cavity surface.
2. In a separate calculation, the detailed shield is modeled without any representation of the microreactor core. Vacuum boundary conditions are applied on the external surfaces of the shield to represent no re-entrant particles from outside the shield. The inner shield cavity surface is assigned the surface source from Step 1. A fixed source OpenMC problem is performed using the surface source from the first step to tally neutron-gamma heating inside the shield.
3. The heat source inside the shield from OpenMC is transferred to the thermal model of the shield using Cardinal's data transfer capabilities. The temperature field inside the shield is then calculated using the heat transfer module in MOOSE.

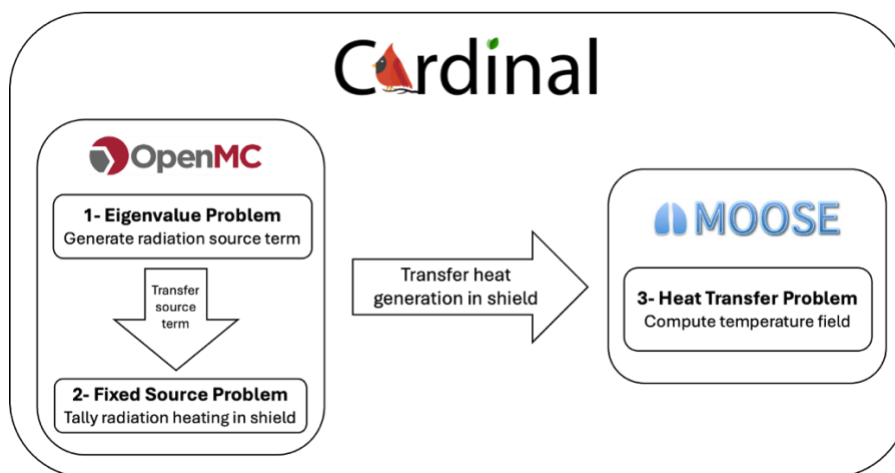


Figure 2-3. Proposed multistep computational workflow of DOME shield neutronics and thermal calculations under MOOSE framework.

The following subsections detail the OpenMC model, the thermal model, the coupled Cardinal model, and the verification of the workflow for the calculation of the heat source due to neutron and gamma heating.

2.1 OpenMC Reactor Physics Model

In this section, we discuss the reactor physics OpenMC model. The purpose of the reactor physics model is ultimately *to tally neutron and gamma heating distributions in the shield*, which are then provided to the MOOSE thermal model to calculate shield temperature.

Modeling particle transport in a heavily shielded nuclear system such as DOME can prove challenging. Shields are designed specifically to prevent particles from passing all the way through them. Numerically, this means that shielding calculations using Monte Carlo particle samples will require substantially more particle histories (e.g., increasing the number of particles and cycles) or the use of variance reduction techniques (e.g., weight windows) to obtain acceptable statistics on tallies located deep within or outside the shield (e.g., dose rate, deposited heat). One possible approach to improve the precision of tally results in shielding calculations is to divide the calculation into two successive steps where particles crossing a specific surface in the first step are used as the source of the second step.

We recall that several major goals of the computational workflow for computing the DOME shield temperature were to reduce user burden, allow quick updates to the shield geometry, and be computationally efficient. Hence, the two-step reactor physics approach (introduced in Figure 2-3) was initially conceived as a possible way to geometrically isolate the core and shield from each other in separate reactor physics calculations. Using a two-step geometrically isolated neutronics approach would permit a vendor to avoid detailed knowledge of the shield and multiple vendors to re-purpose the official shield model, which would not contain any core information. This geometry separation aspect is particularly beneficial as it decouples the modeling effort of the nuclear reactor and shield design teams by reducing the amount of information to be shared during design iterations.

We now discuss different implementations of the two-step approach on a simplified problem and compare them to a reference one-step (R1S) approach to assess accuracy and understand their limitations.

2.1.1 Reference One-Step Approach

The RS1 approach is the traditional approach where the complete system (core and shield) is modeled together with a single eigenvalue calculation. Figure 2-4 shows a conceptual representation of the DOME model used in the R1S approach. The nuclear reactor core is placed inside the shield which is located inside the facility. The region filling the space between the core and the shield is referred to as a cavity. This approach is considered the reference because no approximations are made with

regards to the system geometry. However, this calculation can be exceedingly expensive due to low particle penetration within the shield and facility, and it also requires detailed knowledge of all major components (core, shield, and facility) by the user.

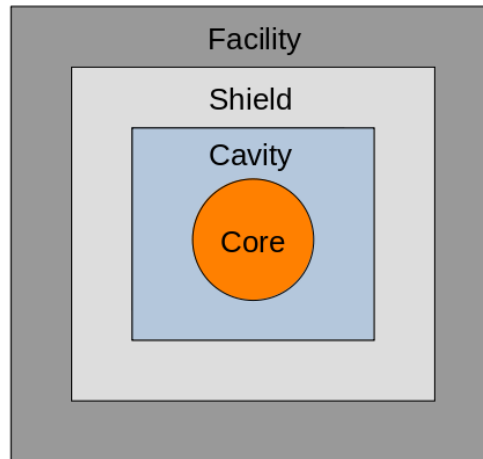


Figure 2-4. Reference one-step approach.

OpenMC generates heating tally information, H , that needs to be converted to physical units, H_{norm} , before transferring to MOOSE heat conduction. With the R1S approach, tally results are normalized using the power of the system and the total heat deposited in the system:

$$H_{norm} = H \times f = H \times \frac{P}{H_{total}}$$

where

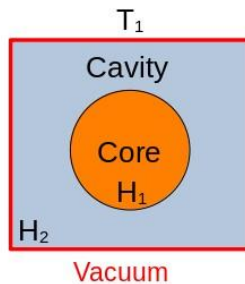
- f [source particle/s]: normalization factor
- P [J/s]: system power
- H [J/source particle]: tallied heat deposited in the shield
- H_{total} [J/source particle]: tallied heat of the total system (core, cavity, shield, facility)
- H_{norm} [J/s]: normalized tally result in physical units

2.1.2 Generic Two-Step Approach

In the generic two-step approach (G2S), the system is geometrically separated into two parts as shown in Figure 2-5. In the **first step**, only the core and cavity are modeled in **an eigenvalue** using a vacuum boundary condition on the outer surface of the cavity to close the system, represented in red. Particles that cross the outer surface of the cavity (the red boundary) are stopped and stored in a bank (e.g., type of particle, energy,

direction, position, weight). In the **second step**, the space inside the shield is modeled as a void region, and the inner surface of the shield, represented in green, is a transmission boundary condition. The bank of particles is used as a source. To close the system in Step 2, the outer surface of the facility is defined as a vacuum boundary condition.

a) Step 1: eigenvalue calculation



b) Step 2: fixed source calculation

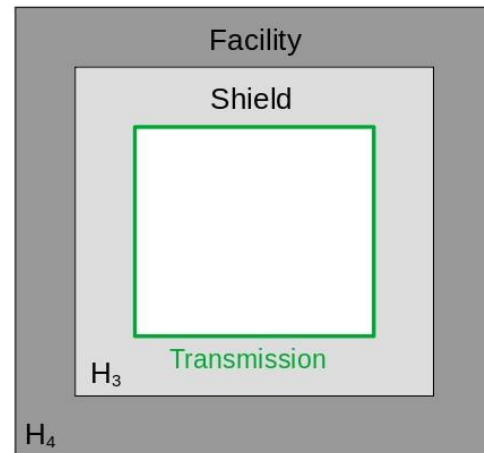


Figure 2-5. Generic two-step approach.

As with other approaches, the G2S approach requires normalization of tally results to physical units before transmitting to MOOSE's heat transfer module. Figure 2-5 shows the variables needed for tally normalization in the G2S approach:

- **H₁** [J/source particle in Step 1]: tallied heat deposited in core
- **H₂** [J/source particle in Step 1]: tallied heat deposited in cavity
- **H₃** [J/source particle in Step 2]: tallied heat deposited in shield
- **H₄** [J/source particle in Step 2]: tallied heat deposited in facility
- **T₁** [particle crossing/source particle in Step 1]: tallied surface current on the outer surface of the cavity in the first step.

OpenMC uses a **filter on T₁** to obtain only the current of particles *leaving the cavity* (not entering the cavity). This surface current tally **T₁** provides a relative magnitude between the tallies in Step 2 and the tallies in Step 1. In practice, the heat deposited in the facility (**H₄**) should be significantly lower than the heat deposited in the other regions and can be neglected.

In the first step, the normalization factor **f₁** [source particle in Step 1 / second] includes the standard heating tallies from both Step 1 and Step 2, where the Step 2 tallies are scaled by **T₁**:

$$f_1 = \frac{P}{H_1 + H_2 + T_1 \times (H_3 + H_4)}$$

For the second step, the normalization factor f_2 [source particle in Step 2 / second] is simply the product of the normalization factor f_1 and the surface current T_1 :

$$f_2 = f_1 \times T_1 = \frac{P \times T_1}{H_1 + H_2 + T_1 \times (H_3 + H_4)}$$

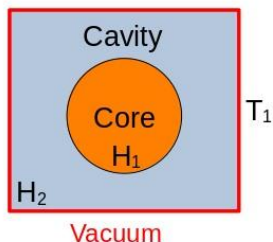
The normalization method requires both steps to be run before any results can be normalized and transmitted to MOOSE thermal heating models.

2.1.3 Enhanced Step 2 Approach: *Enhancing Particle Transport Inside the Cavity in Step 2*

The second step of the G2S approach considers the inner surface of the shield as a transmission boundary condition and the region surrounded by the shield as a void region. Particles scattering back from the shield in Step 2 travel through the void region with no interaction with matter until they re-enter the shield. In the real physical system, particles scattering back from the shield to the cavity are expected to interact with materials inside the cavity region and core. Depending on several factors (geometric aspect ratio, physical properties of the cavity, and core materials), the backscattered particles can either be absorbed in the core or in the cavity or can scatter again and reach the shield another time.

The second step of the method can be modified to more accurately model the physics by running the fixed source calculation on the complete system as in Figure 2-6(b). While this modification does not allow a strict geometric separation between the two steps, it provides the most exact way of modeling particle transport in the second step. In practice, the creation of fission neutrons in the fissile material of the core should be turned off during the fixed source calculation in Step 2.

a) Step 1: eigenvalue calculation



b) Step 2: fixed source calculation

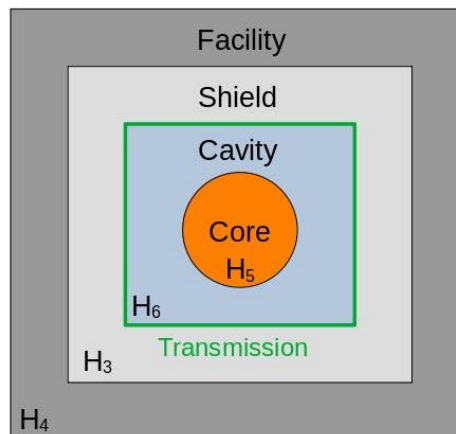


Figure 2-6. Enhanced Step 2 approach.

The Enhanced Step 2 (ES2) approach follows a similar normalization approach as the G2S approach except that the heat deposited in the core and the cavity in the second step should also be accounted for in the total heating used for normalization as represented in the following equation:

$$f_2 = f_1 \times T_1 = \frac{P \times T_1}{H_1 + H_2 + T_1 \times (H_3 + H_4 + H_5 + H_6)}$$

Figure 2-6 shows the new variables needed for tally normalization in the ES2 approach:

- **H₅** [J/source particle in Step 2]: tallied heat deposited in core from Step 2
- **H₆** [J/source particle in Step 2]: tallied heat deposited in cavity from Step 2.

Variations of the ES2 approach can also be considered to limit the degree of accuracy in representing the core in Step 2. These variations include the use of vacuum or reflective boundary conditions on a surface surrounding the core, using a homogeneous material with a finely tuned absorption property in the cavity or using reflective boundary conditions on the inner surface of the shield in Step 2. All those variations are approximations of the ES2 approach and generally require the results of a reference calculation to determine their accuracy.

2.1.4 Enhanced Step 1 Approach: *Accounting for Reactivity Feedback in Step 1*

The Step 1 eigenvalue calculation of the G2S approach cannot simulate particles re-entering the core after interacting with the shield. The vacuum boundary condition located on the outer surface of the cavity prevents any particle that reaches the surface from being transported further. This limitation can negatively impact the core reactivity as the leakage fraction is artificially increased, resulting in a potentially biased estimate of the heat in the shield.

The Enhanced Step 1 (ES1) approach addresses this issue by modeling the entire system in Step 1 as shown in Figure 2-7(a). A transmission boundary condition on the outer surface of the cavity in Step 1 allows particles to re-enter the core from the shield. Only the particles coming from the cavity cell are banked on the outer surface of the cavity. With this approach, the only acceptable boundary condition for the inner surface of the shield in Step 2 is vacuum. The surface source bank from Step 1 and the surface current T_1 , which are used for normalization, now account for multiple re-entrances in the shield. For example, a particle that entered the shield twice during its lifetime will be stored in the surface source bank as two distinct particles (if the size limit of the bank is not reached before). For this same example, the surface current T_1 will see two particles crossing the surface for one generated particle. Therefore, particles should be stopped at the inner surface of the shield in Step 2 to avoid overestimating the total travel length of particles in the shield. The ES1 approach follows the same normalization method as the one described for the G2S approach. Limitations of the ES1 approach are discussed in Appendix A.

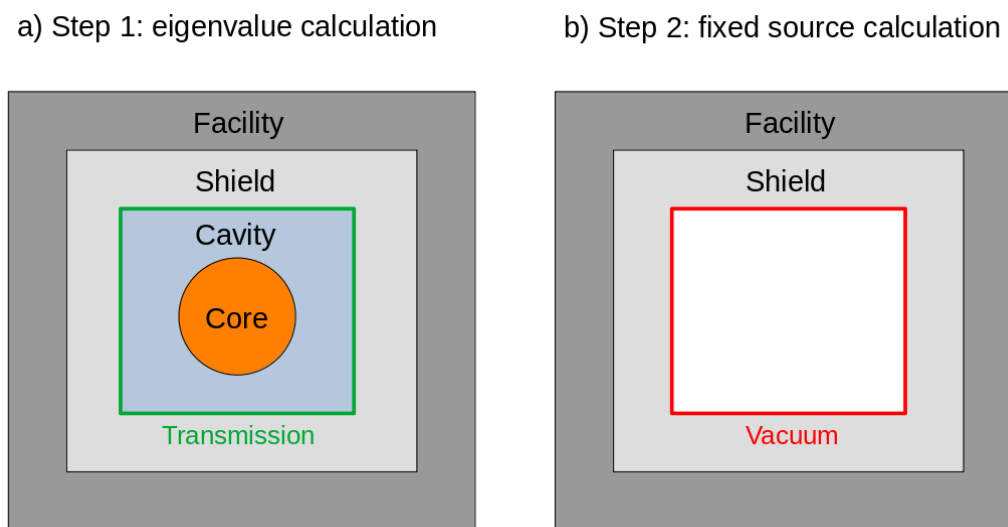


Figure 2-7. Enhanced Step 1 approach.

The ES1 approach does not allow a strict geometric separation of the two steps but can potentially be adjusted to avoid modeling the entire shield and facility. This variation of the ES1 approach consists in only representing a fraction of the shield surrounding the cavity in Step 1 so that enough backscattered particles are simulated to be representative of the complete model. The main challenge with this approach is to evaluate how the geometric approximation can be done (changing the thickness, the material composition or the density of the shield). Reference calculations using the R1S approach will be needed to validate this variation of the ES1 approach.

2.1.5 Comparison of approaches for simplified geometry

The various two-step approaches (G2S, ES2, ES1), summarized in Table 1, are compared against the reference one-step model (R1S) using a simplified spherical model of the DOME shield Figure 2-8.

Table 1. Summary of investigated approaches

Approach Acronym	Approach Name	Step 1 Description	Step 2 Description
R1S	Reference one-step	Core-cavity + shield	-
G2S	Generic two-step	Core-cavity only	Shield only
ES2	Enhanced Step 2	Core-cavity only	Core-cavity + shield
ES1	Enhanced Step 1	Core-cavity + shield	Shield only

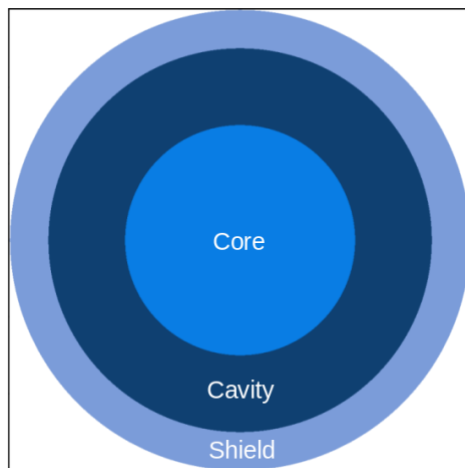


Figure 2-8. Simplified OpenMC model.

All calculations are performed using OpenMC version 0.15.0 [8] and nuclear data from the ENDF/B-VIII.0 library [9]. OpenMC uses coupled neutron-photon transport in every calculation. Every eigenvalue calculation is run with 100,000 particles using 15 inactive and 35 active cycles. The surface source banks produced in the first step of the two-step approaches have a maximum capacity of 1,000,000 particles. Every fixed source calculation is run with 1,000,000 particles using 50 batches. Results presented in this section use the 1σ uncertainty from OpenMC.

The spherical core has a radius of 30 cm and is filled with a homogeneous mixture of water at a density of 1 g/cm³ and uranium dioxide at a density of 10.97 g/cm³ enriched at 5 wt% in uranium-235. The composition of this mixture is equivalent to the composition of a rectangular pressurized-water reactor lattice with a rod radius of 0.49 cm and a pitch of 1.26 cm. Thermal scattering data associated with hydrogen in water are used for this homogeneous mixture. The inner and outer surfaces of the shield have a radius of 50 and 60 cm, respectively. The cavity between the core and the shield is filled with air at a density of 0.001225 g/cm³. The shield is also filled with air and its density is varied (0.1, 0.2, 0.4, 0.6, 1.0, 1.5, and 2.0 g/cm³) to represent multiple backscattering probability regimes. When the shield density is low, particles are more likely to escape the system. Conversely, when the shield density is higher, more particles are expected to scatter back from the shield to the core. To quantify the backscattering probability regime of the system, a backscattering current ratio is evaluated from the reference calculations performed with the R1S approach. The backscattering current ratio is calculated from the ratio of two surface current tallies defined at the inner surface of the shield:

$$\text{Backscattering current ratio} = \left| \frac{C_{\text{back}}}{C_{\text{forward}}} \right|,$$

where C_{back} is the surface current of particles coming from the shield and C_{forward} is the surface current of particles coming from the cavity.

Figure 2-9 shows the difference in pcm between the k_{eff} values of a given approach and the R1S approach:

$$k_{\text{eff difference}} = |k_{\text{eff}} - k_{\text{eff,R1S}}|,$$

The G2S and ES2 approaches share the same eigenvalue calculation in Step 1, so their results are identical. Similarly, the R1S and ES1 approaches use the same model in their eigenvalue calculation which results in no difference in k_{eff} values. As theoretically expected, Figure 2-9 illustrates that the GS2 and ES2 approaches fail to capture the impact on the core reactivity of particles that would normally scatter back to the core if the shield was modeled. For G2S and ES2, k_{eff} errors are minimal for low backscattering current ratio but become severe for larger backscattering current ratios.

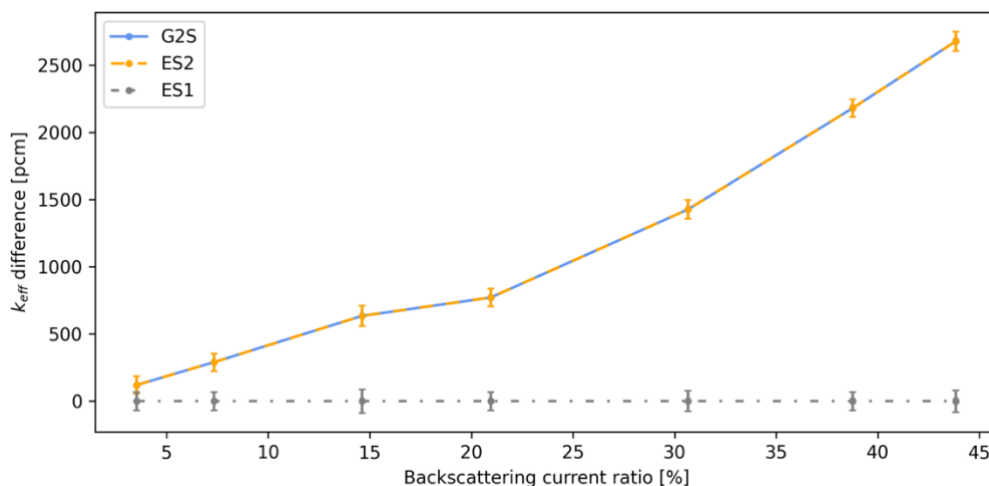


Figure 2-9. Difference in keff between the reference and two-step approach variations for different backscattering current ratios.

Figure 2-10 plots the relative difference in heating between a given approach and the R1S approach calculated with:

$$\text{Heating relative difference} = \left| \frac{H - H_{R1S}}{H_{R1S}} \right|,$$

where **H** is the heat deposited in the shield retrieved from the second step of the G2S, ES2 or ES1 approach and **H_{R1S}** is the heat deposited in the shield obtained from the R1S approach. For low backscattering current ratios (<10%), all the approaches proposed in this analysis are relatively close (< 5%) to the reference approach in terms of shield heating. The ES2 approach performs particularly well compared to the ES1 approach when the backscattering current ratio is still relatively low (<15%). When the backscattering effect becomes more important, the ES1 approach provides the best results compared to the G2S and ES2 approaches. The results obtained with the ES1 approach do not vary significantly with the backscattering current ratio and stay under 5% difference from the reference, while the errors for the G2S and ES2 increase almost linearly with the backscattering current ratio.

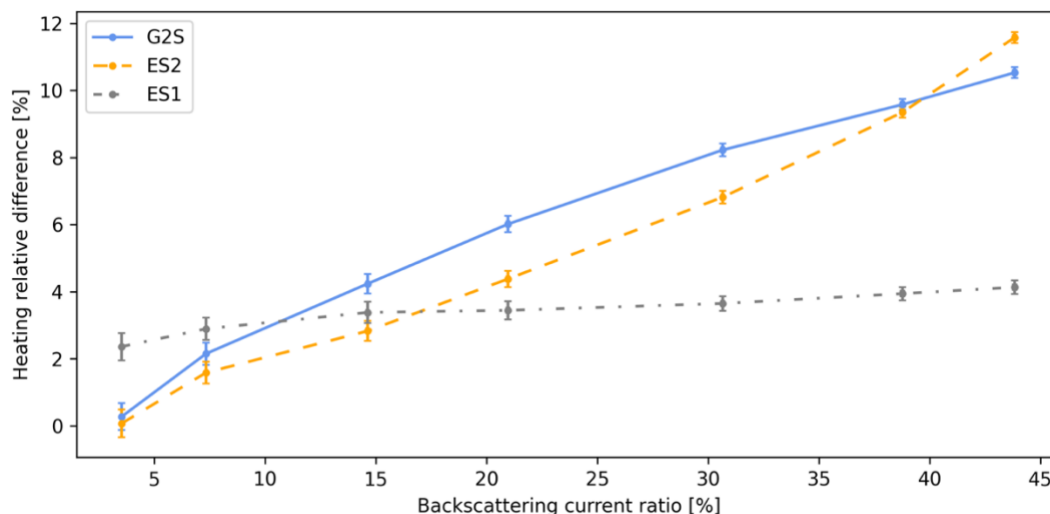


Figure 2-10. Relative difference in heat deposited in the shield between the reference and two-step approach variations for different backscattering current ratios.

2.1.6 Recommendations on Selecting of a Two-Step Approach

While the G2S approach provides a strict geometric separation between each model of the two steps, it cannot account for the reactivity feedback due to backscattered particles re-entering the core in the real system. Additionally, particle transport cannot be accurately modeled in the second step of the G2S approach as no model is represented inside the cavity. Two different enhancements of the generic approach were proposed, which both come with the cost of losing the strict geometric separation. The Enhanced Step 2 (ES2) approach consists of modeling the complete system in the second step so that particle transport is correctly simulated. Like the G2S approach, the ES2 approach suffers from not taking into account the reactivity feedback of backscattered particles on the core reactivity, which can lead to an important bias in the shield heating estimation when the backscattering current ratio is high. The Enhanced Step 1 (ES1) approach consists of modeling the complete system in the first step so that backscattered particles are taken into account in the eigenvalue calculation. *Based on an analysis with a simplified geometry, the choice of the best two-step approach depends on the backscattering probability regime.* The ES2 approach performs better with low backscattering current ratios while the ES1 approach performs better when the backscattering current ratio is high. This makes the ES1 approach particularly adapted for reactors with a high leakage fraction such as a reactor with no individual shield surrounding it. *Regardless of backscattering current ratio, the ES1 approach seems to be the more robust option with no significant variations in the heating compared to a R1S calculation.*

To determine which workflow is optimal for a specific vendor design, it is recommended to first evaluate the backscattering probability regime (i.e., backscattering

current ratio). Three options to evaluate this regime are given in order of increasing modeling and computing complexity:

- Retrieve the leakage ratio of an eigenvalue calculation of the reactor core being considered
- Modify the Step 1 calculation of the G2S approach to replace the vacuum boundary condition by a pure reflective boundary condition and evaluate the impact on the core reactivity
- Run a complete eigenvalue calculation following the R1S approach.

If the expected backscattering current ratio is low, any of the enhanced two-step approaches (ES2 or ES1) should give reasonable results for the heat deposited in the shield but the ES2 approach could be the better option. While the G2S approach could potentially be used in that case, the proposed analysis does not provide a metric to quantify the impact of not modeling particle transport correctly in the second step. *If the expected backscattering current ratio is not known or is relatively high, the ES1 approach should be used preferably.* In any case, having access to a reference calculation using the R1S approach would be the best option to evaluate which of the enhanced options is the best fit for a given application and geometry.

Three variations of the enhanced approaches present potential advantages that could be investigated further. However, the main drawback of these variations is that they require a reference calculation to determine a parameter of interest. The first variation is to use the ES1 approach with a simplified shield layer in the first step to avoid modeling the whole system. The shield simplification can take the form of using only a thin layer of the complete model. Comparison to a reference calculation would be needed to determine the minimal thickness required to capture the backscattering effect correctly. The two other variations are both based on the use of reflective boundary conditions instead of the transmission boundary condition used in Step 2 and Step 1 of the ES2 and ES1 approach, respectively. The advantage of these variations is to conserve the geometric separation of the G2S approach. The challenge of using reflective boundary conditions is to determine the correct albedo factors.

The generic two-step approach will be adopted to develop the DOME microreactor and shield base model because it features a clear separation between the microreactor and the shield calculations and is the less computationally expensive. The reference 1-step method will be used to verify the G2S is appropriate, and the enhanced two-step approaches will be compared to the G2S to demonstrate they can be attractive alternatives if the errors generated by the G2S are too large.

2.1.7 OpenMC Models of the DOME Microreactor and Shield using the Generic Two-Step Approach

We now discuss the specific details of the OpenMC model for the microreactor and shield used in this demonstration. We first explore the G2S approach by modeling a

microreactor with vacuum boundary conditions imposed at the surfaces of the shield cavity, followed by a fixed source problem using the surface source from the first step.

We leverage an open-source microreactor model (in place of a proprietary industry concept) based on the Benchmark Assessment (SiMBA) problem [6]. Figure 2-11 shows an axial view (x-z slice) of the core. The inner radius of the core vessel is 107.0 cm and its height is 120.0 cm. The core consists of 18 hexagonal assemblies each containing 96 fuel pins of radius 0.5 cm and height 100.0 cm, 60 Yttrium Hydride (YH_x) pins of radius 0.475 cm and height 100.0 cm, and 61 sodium heat pipes of radius 0.9 cm and height 120.0 cm drilled into a graphite monolith. The core vessel is filled with beryllium reflector around the assemblies from all sides.

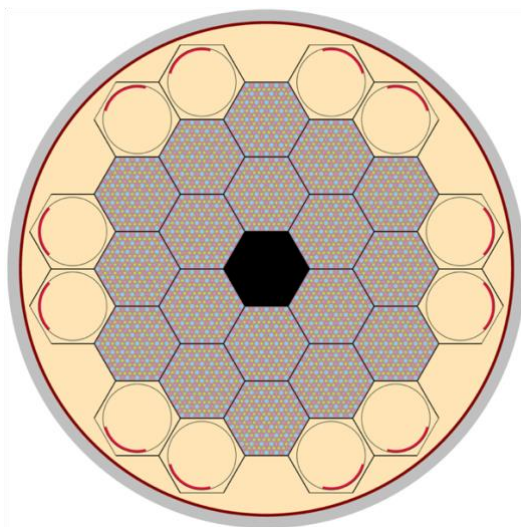


Figure 2-11. Cross-sectional view of microreactor OpenMC model (x-z slice).

The core is placed in the horizontal direction inside the shield cavity with the reactor axis coincident with the y-axis, as shown in Figure 2-11. The heat pipes penetrate the reflector above the core on the side facing the water tank only, making the reactor asymmetric along the y-axis. The core vessel is made of 2.0 inch stainless steel lined from inside with a 0.5 inch Tungsten Tetraboride WB_4 shielding layer to attenuate the radiation reaching the DOME shield. A view of the reactor within the DOME shield is shown in Figure 2-12.

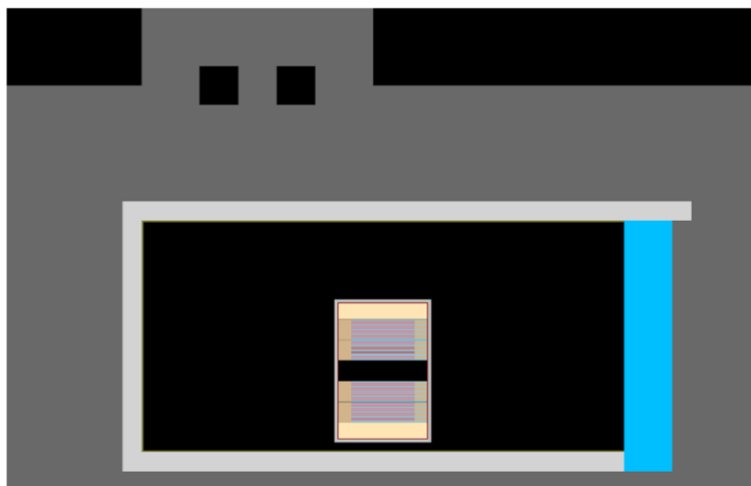


Figure 2-12. Axial view of combined reactor and shield OpenMC models.

Step 1 – Eigenvalue problem results: The OpenMC eigenvalue problem of the reactor alone was simulated using 500 active batches, 50 inactive batches, and 10^6 particles per batch. The maximum error in the heating tallies was less than 0.0002. The k_{eff} of the reactor is 1.10750 ± 0.00005 . Figure 2-13 compares the neutron and photon fluxes at the reactor boundaries to the shield operational flux specification from Reference [2]. Figure 2-14 shows the flux distribution in the shield cavity.

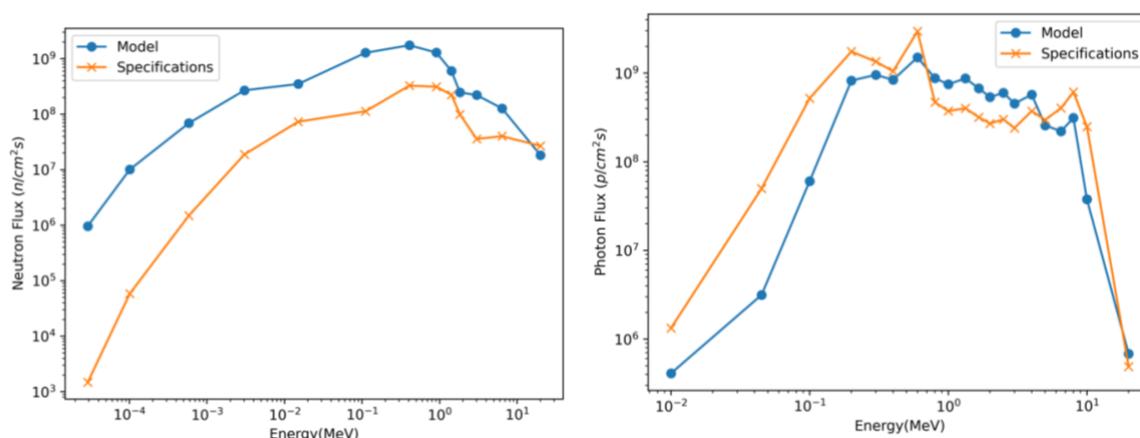


Figure 2-13. Neutron and gamma fluxes compared to the specification.

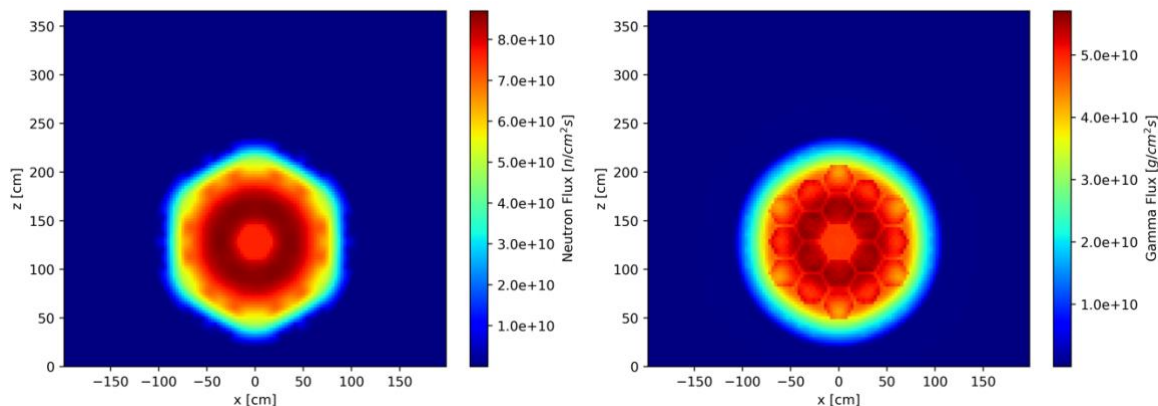


Figure 2-14. Neutron and gamma fluxes for the eigenvalue problem.

Step 2 – Fixed source problem results: The source intensity for the fixed source problem (Step 2) was computed from the eigenvalue value problem (Step 1) using the normalization described in Section 2.1.2. The fixed source problem was simulated using 10^{10} particles. Figure 2-15 shows the neutron flux, gamma flux, and heat rate distributions inside the shield. Each figure is a 2D plot of one of the designated quantities averaged on the third axis.

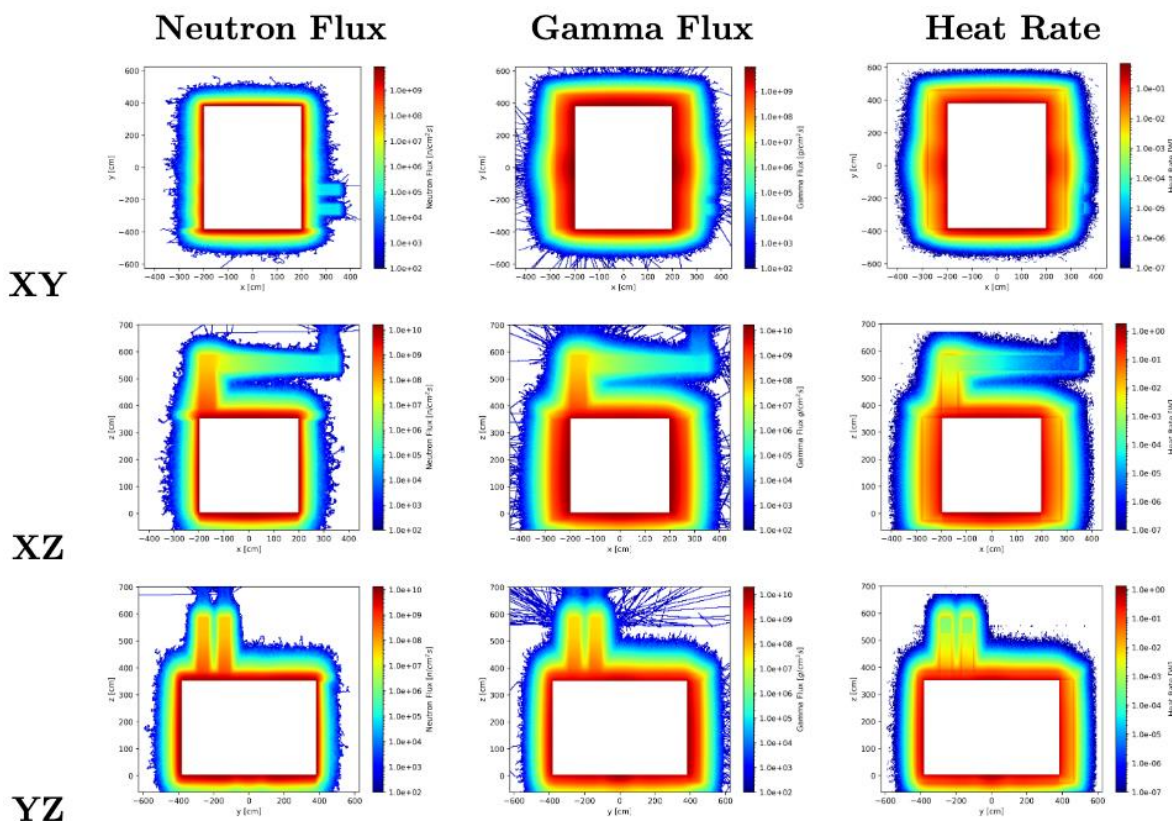


Figure 2-15. Neutron and gamma fluxes and heat rate in the DOME shield for the fixed source problem.

The total heat source inside the shield was 3.5 kW with the distribution shown in Table 2. This highlights the role of the water tank in the shielding system by redirecting a substantial portion of the heat away from the concrete, thereby helping to lower the maximum temperature in the concrete due to neutron-gamma heating.

Table 2. Heat source distribution within the shield.

Region	Heat source (kW)	Fraction of heat source (%)
Ordinary concrete	1.670	47.7
Magnetite concrete	0.371	10.6
Water tank	1.267	36.2
Insulation layers	0.189	5.4
Ground	0.003	0.1
Total	3.500	100

2.1.8 Comparison of approaches for DOME shield model

The results obtained in Section 2.1.7 leveraged the generic two-step approach (G2S). Various other two-step approaches were also used to calculate the heat source from neutron and gamma heating and compare this result and the R1S calculation.

Table 3 summarizes the heat source computed by OpenMC in the shielding region for the different one- and two-step approaches. It should be noted that the leakage fraction of particles leaving the core and entering the shielding region is ~2%, which represents a regime with a relatively small fraction of source particles reaching the shielding region. Note that the model used for this verification is slightly different than the model presented in the previous section, resulting in a different heat rate, but these differences do not affect the conclusion of this verification.

Table 3. Comparison of heat source in the shielding region comparing various OpenMC one- and two-step modeling approaches.

Approach	Heat source computed in shielding region (kW)	Percent Error vs. R1S (%)
R1S	3.320	-
G2S, with step 2 vacuum b.c.	2.613	-21.29
G2S, with step 2 transmission b.c.	3.620	9.04
ES2	3.382	1.87
ES2-black absorber	3.400	2.41
ES1	3.317	-0.08

The results shown in Table 3 confirm that the G2S has significant error in the heat source tallied in the shielding region in the Step 2 calculation, whether a transmission or a vacuum boundary condition is used in the step 2 calculation. This error is the result of ignoring significant backscattering from the shielding region back into the core region. Since the first step of the G2S approach stops the particle history and banks the source particle immediately at the initial surface crossing between the core and shielding region, backscattering effects that would normally happen in the reference solution do not get modeled in this scenario. Based on this particular core and shielding design, neglecting this effect can cause significant differences in the total heat source computed in the shielding region. It should be noted here that the total shielding heat source is used to normalize the heat source within each spatial tally zone. Thus, any biases in this value will have direct effects on the heat source for each spatial zone of interest within the shielding region as well. When a vacuum boundary condition is used in the Step 2 calculation, the heat source is underpredicted (i.e. amount of backscattering into the core is also underpredicted), and when a transmission boundary condition is used, the heat source is overpredicted (i.e. amount of backscattering into the core is also overpredicted).

The ES2 approach provides a workaround for this, where the second step of the two-step approach models the core region explicitly (ES2 approach) or as a pure black absorber region (ES2-black absorber approach). In these approaches, some or all of the core is modeled in the fixed source calculation. While there is still some residual error with using such an approach, this brings the heat source error much closer to the reference value than the naïve GS2 approach.

The ES1 approach produces the most accurate results for the heat source predicted in the shielding region. This accuracy comes from the fact that the surface source used in the Step 2 calculation accounts for all particles that crossed the core-shielding boundary, regardless of whether these particles originated from the core region or were backscattered from the shielding region. The downside of this approach is that it requires a full one-step calculation (core + shielding) in the step 1 eigenvalue calculation. Thus, the Step 1 eigenvalue core calculation is no longer decoupled from the Step 2 shielding fixed source calculation. It may still offer benefits over the R1S method in terms of variance reduction deep in the shield as well as being able to leverage a shield-only model for the heating calculation (Step 2).

2.2 MOOSE Thermal Model

The DOME thermal model utilizes the MOOSE heat transfer module to calculate the shield concrete temperature distribution. Figure 2-16 shows the mesh of the thermal model, which was generated using MOOSE. In particular, the mesh of the insulation layers was meticulously generated to ensure conformality with the coarser mesh in the concrete, as shown in Figure 2-17. The mesh element size in the concrete is 0.5 ft.

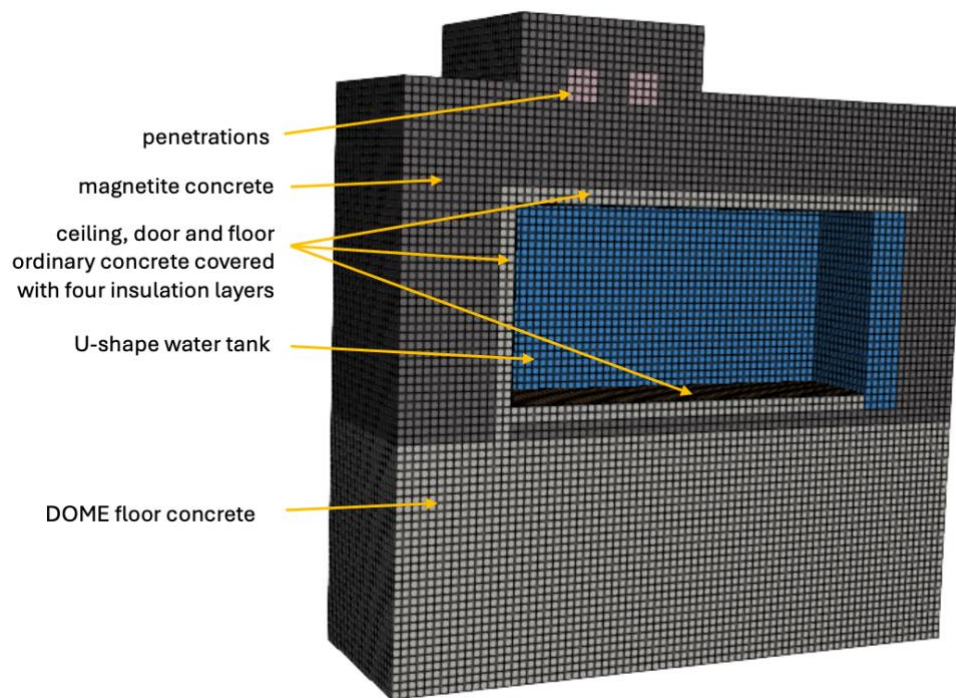


Figure 2-16. Computational mesh used for the heat transfer model.

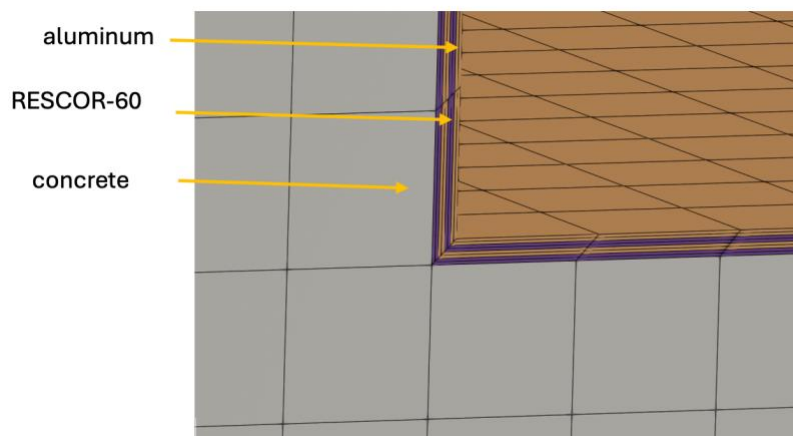


Figure 2-17. Mesh details of the insulation layers covering the floor, doors and ceiling.

The core is assumed to be a box inside the shield cavity (in red in Figure 2-18). Contacts between the core and the shield are assumed to be very small and neglected. There is a 0.5 ft clearance between the reactor box and the shield floor.

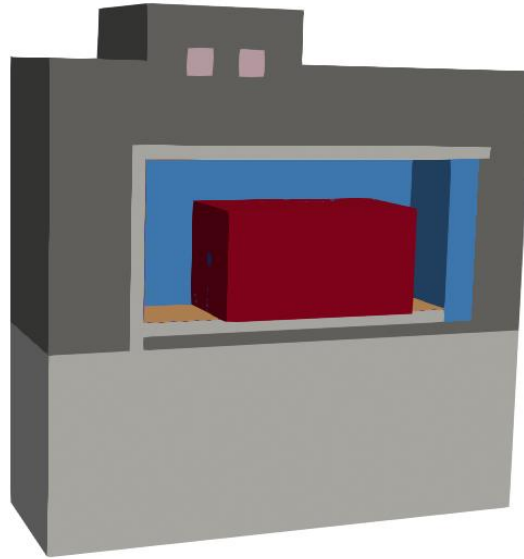


Figure 2-18. Thermal model geometry including the reactor box.

The thermal model is developed using the following assumptions and boundary conditions:

- The main mechanisms for heat transfer between the reactor vessel and the shield inner surface are radiation, natural convection, and conduction through air. This is justified by the fact that the support structure would have a small footprint and direct heat conduction would be very small.
- The heat rate released from the reactor to the shield is 50 kW. This value was used for the conceptual design in Reference [2]. This assumption is needed because most of the heat is transported out of the reactor vessel by the primary coolant system which is not explicitly modeled here.
- The temperature of the water in the U-shaped water tank is assumed to be constant at 300 K. The water will be cooled with a flow pattern that is unknown at this time but will maintain a maximum outlet temperature of 300 K (80°F). Thus, the water will be modeled as a solid with an artificially high thermal conductivity and a fixed temperature boundary condition at the bottom of the tank.
- A convective boundary condition with a constant heat transfer coefficient of 10.0 W/m².K and an ambient temperature of 300 K is used on the outer surfaces of the shield in contact with the atmosphere. The value of the heat transfer coefficient will be verified with a sensitivity analysis.
- The bottom surface of the shield is extended by 15 ft to represent the ground beneath the structures, with adiabatic boundary conditions applied.
- The emissivity of the reactor box is assumed to be 0.6, which is consistent with stainless steel. The emissivity of the water tank (assumed to be painted in black) is 0.98, and a value of 0.04 is used for the aluminum surfaces. These values are taken from the conceptual design report [2].

- Material properties for ordinary concrete, water, aluminum, insulation and air are taken from Reference [2]. The properties of the high-density concrete were not defined and were assumed based on values from literature. Note that in Reference [2], the magnetite concrete was modeled as ordinary concrete. The thermal conductivity of air was set as a temperature-dependent function at atmospheric pressure. The resulting material properties are summarized in Table 4.
- Similar to the assumption made in Reference [2], the thermal conductivity in the cavity is set to 0.5 W/m.K to account for natural convection in the cavity.

Table 4. Material properties used in the thermal model

Material	Density [kg/m ³]	Thermal conductivity [W/m.K]	Specific heat [J/kg.K]
Air	1.16	Temperature dependent	1050
Aluminum	2,270	175	875
Ordinary concrete	2,403	0.75	1050
Magnetite high-density concrete	3,524	5 (assumed)	1050
RESCOR-60 insulation	256	0.065	1047
Stainless steel-304	7,850	60.5	434
Water	988	6000 (see assumption above)	4184

2.2.1 Base Thermal Model Results

Using the conditions above, and not accounting for the neutron and gamma heating, the maximum temperature in the concrete is 77°C with the temperature distribution shown in Figure 2-19. The highest temperatures are observed in the floor center and on the ceiling and doors. We can verify that the temperature is constant in the water tank, showing that the thermal conductivity has been adjusted to a sufficiently high value.

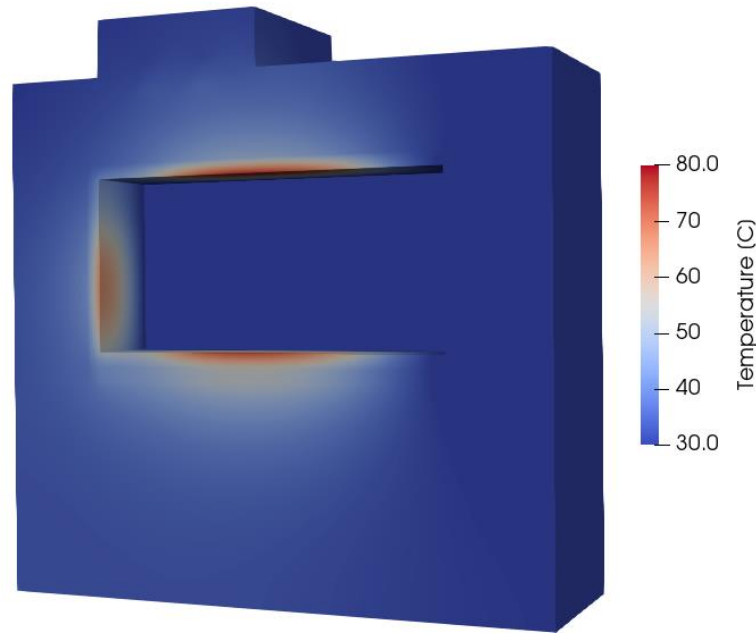
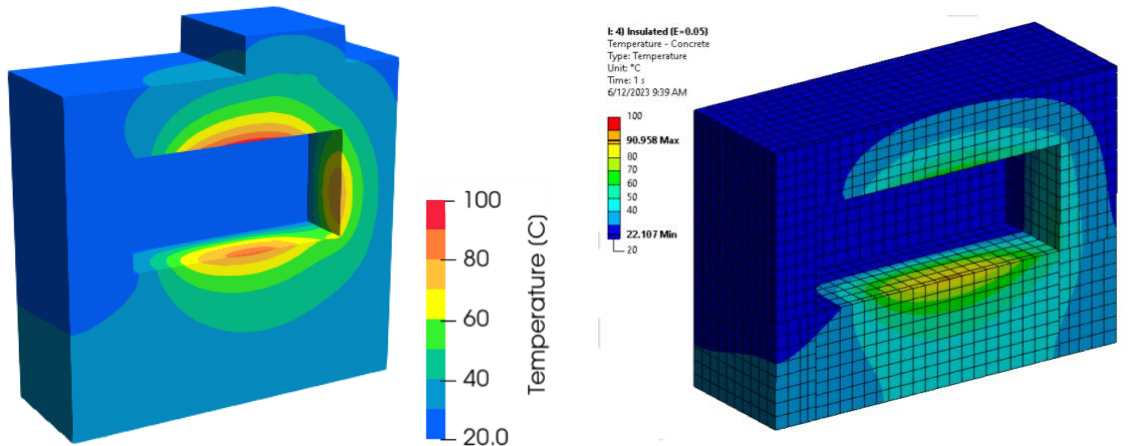


Figure 2-19. Temperature distribution in the concrete for the thermal base model.

2.2.2 Comparison with the ANSYS Model

In the conceptual report [2], the thermal analysis was conducted using ANSYS. The higher thermal conductivity of the high-density concrete was not accounted for, leading to a higher maximum temperature distribution. This assumption was implemented in the thermal model to verify similar results would be obtained. Figure 2-20 shows the temperature distribution in the concrete for each model. Note that the color scale was adjusted to be similar but is not exactly the same. The ANSYS maximum temperature is 91°C while the MOOSE thermal model predicts a maximum temperature of 94.8°C. This difference can be explained by the implementation of the radiative heat transfer in the MOOSE model, which only imposes the heat flux on reactor projected area of the reactor on the shield faces instead of the whole surface. This is leading to an overprediction of the temperature. More accurate view factors will be implemented in the next version of this model.



MOOSE model

ANSYS model [2]

Figure 2-20. Comparison of the MOOSE and ANSYS thermal models.

2.2.3 Sensitivity Analysis

To validate the assumptions made when developing the thermal model, a sensitivity analysis of the maximum temperature with respect to various parameters is performed.

Mesh: A mesh sensitivity analysis is performed to verify that the mesh size is appropriate. The base mesh has two elements per linear foot. A coarser mesh with one element per foot and a finer mesh with four elements per foot were used to compare with the base case. The results are shown in Figure 2-21. There is a 0.3 K difference between the coarser and base meshes. The difference is 0.03 K between the fine and base meshes. This demonstrates that the base mesh is optimally refined.

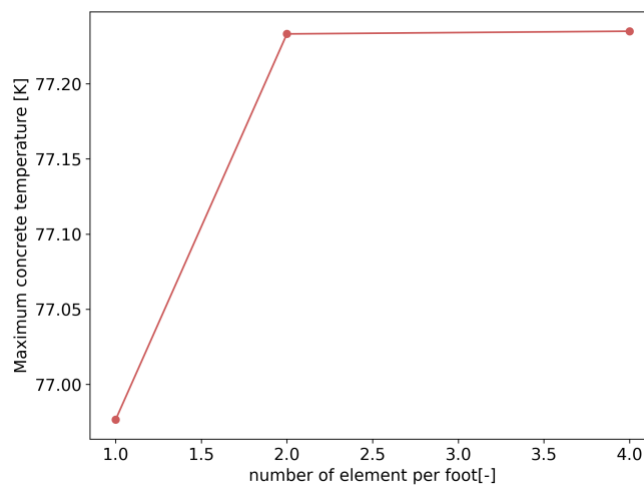


Figure 2-21. Mesh sensitivity for the thermal model.

Cavity thermal conductivity: The cavity thermal conductivity is tuned to 0.5 W/m.K following the recommendation in the conceptual design report. A sensitivity analysis on this value was performed, and the results are shown in Figure 2-22. Values between 0.1 and 0.7 W/m.K show a temperature variation of -3 K to +4 K.

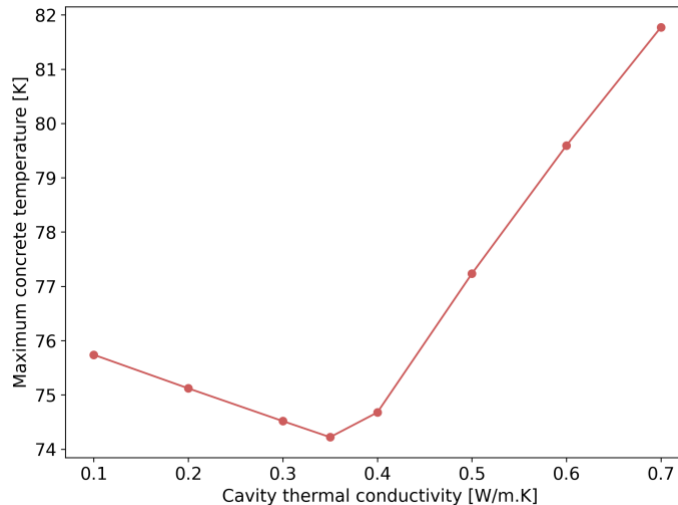


Figure 2-22. Sensitivity analysis of the maximum concrete temperature with respect to the cavity thermal conductivity.

Reactor clearance: The reactor position inside the cavity may vary. In the base case, the distance between the reactor and the shield floor is 0.5 ft. If it is set to 1 ft, the maximum concrete temperature increases by 2 K because the maximum shifted from the floor to the ceiling.

Reactor emissivity: The condition of the reactor surface, and consequently its emissivity, may vary from one reactor design to another. The sensitivity of the maximum concrete temperature with respect to the emissivity is shown in Figure 2-23.

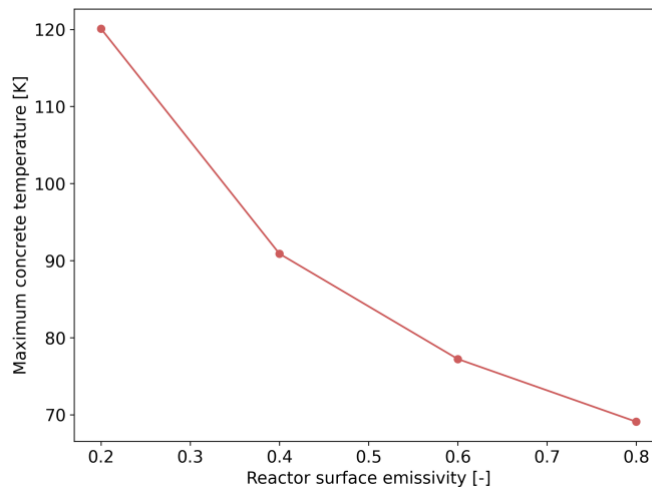


Figure 2-23. Sensitivity analysis of the maximum concrete temperature with respect to the reactor surface emissivity.

Convective boundary condition with environment: The heat transfer coefficient for the convective heat transfer between the shield outer surface and the environment was modified from 1 W/m².K to 10 W/m².K. The maximum concrete temperature decreased by 2 K.

Reactor heat distribution: The heat source in the reactor is uniform in the base model. A sensitivity case where the heat source is applied only to a 2.5-ft-radius and 13-ft-long inner cylinder was performed showing an increase of 0.5 K.

In conclusion, among all the parameters studied, the reactor emissivity value has the most important impact on the maximum concrete temperature.

2.3 Cardinal Model

The coupled Cardinal [3] simulation allows for calculating the temperature profile within the shielding region, using the heat source from the shielding region directly calculated by OpenMC for the neutron and gamma heating. Cardinal bridges the MOOSE thermal model described in Section 2.2 and the OpenMC model described in Section 2.1. Cardinal operates by initiating a call to OpenMC to run a neutronics solve. Once this solve has completed, Cardinal transfers the calculated heat source from OpenMC to the MOOSE thermal model by mapping the heat source in the OpenMC cells that comprise of the shielding region to their analogous locations in the finite element mesh used by the MOOSE thermal model. This transferred heat source acts as the initial heat source assumed in the MOOSE thermal model for the shielding region, and a thermal physics solve is initiated. A consistent geometry needs to be defined between the OpenMC and MOOSE thermal models to ensure that Cardinal correctly maps the heat source between these two codes. For the purposes of this work, this heat source transfer occurs only as a one-way transfer from OpenMC to MOOSE. Calculated temperature profiles from MOOSE can be fed back into OpenMC to establish a fully coupled neutronics-thermal physics simulation, but this is left as future work.

2.3.1 Coupled Cardinal Simulation Results Using the Generic Two-Step approach

The coupled simulation has been run using the G2S approach to generate the heat rates. The resulting power distribution in the DOME shield from neutron and gamma heating is shown in Figure 2-24.

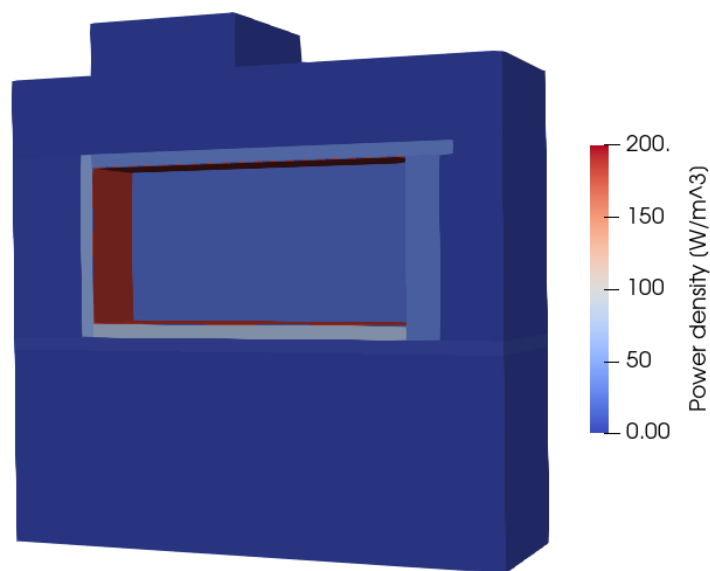


Figure 2-24. Power density in the DOME shield due to neutron and gamma heating.

Including this additional neutron and gamma heating source in the MOOSE thermal model results in an increase of the peak concrete temperature in the DOME shield from 77 C to 84°C. The temperature distribution for the coupled model is shown in Figure 2-25.

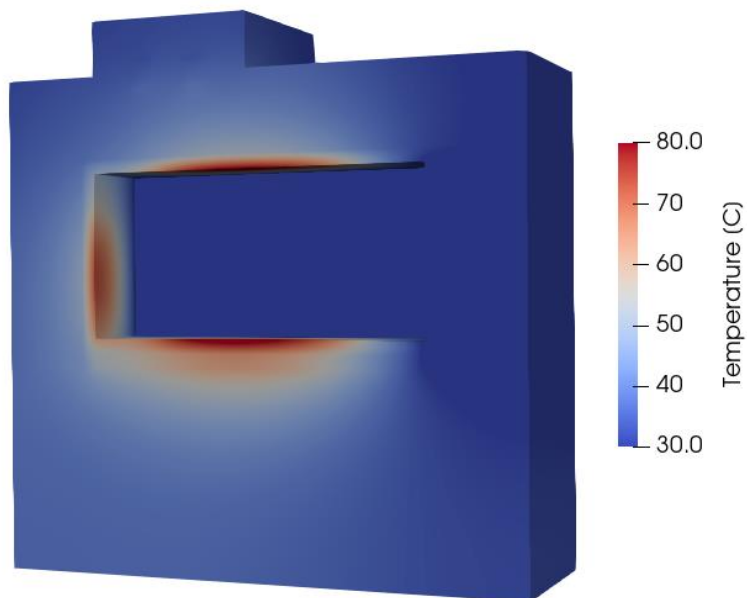


Figure 2-25. Temperature in the DOME shield due to neutron and gamma heating.

2.3.2 Comparison of Approaches for Cardinal model of DOME Shield Model

In Section 2.1.8, we examined the impact of various two-step approaches on the heat source computed by OpenMC. We now extend this comparison to examine the impact of various two-step approaches on the final Cardinal-computed temperatures in the shield, which is our quantity of interest. Table 5 shows the peak concrete temperature predicted within the shielding region with each approach. Note that the model used for this verification is slightly different than the model presented in the previous section, but these differences do not affect the conclusion of this verification.

Table 5. Comparison of peak concrete temperature in shielding region comparing various OpenMC one- and two-step modeling approaches.

Approach	Peak Concrete Temperature (°C)	Percent Error vs. R1S (%)
R1S	79.0	-
G2S, with step 2 vacuum b.c.	77.9	-1.4
G2S, with step 2 transmission b.c.	79.4	0.5
ES2	79.1	0.1
ES2-black absorber	79.1	0.1
ES1	79.0	0.0

The magnitudes of the errors in the peak concrete temperature follow the same trends as the errors in the OpenMC heat source shown in Table 3, where an over- and underprediction of the OpenMC heat source leads to an over- and underprediction of the maximum concrete temperature. When focusing on just the temperature profile, the relative differences in the peak concrete temperatures do not have a very large magnitude when compared to the reference peak temperature. However, it should be noted that these results may be highly dependent on the specific core conditions and specifications, and it is recommended for any vendor pursuing a similar two-step calculation to make sure that significant deviations do not exist between the one- and two-step calculations for the particular core and shielding conditions under consideration. Further work is needed to understand how changing the core design and operating conditions will affect these temperature comparisons.

In conclusion, a number of alternatives have been proposed for the specific case where a G2S approach shows significant deviation from a R1S approach. This effect is most likely caused by the significant effect of backscattering from the shielding back into the core region, which a naïve two-step approach would not be able to adequately capture. Three potential solutions are provided and work well, specifically for the DOME model with this microreactor concept:

- Option 1: Pursue ES1, which ensures that the surface source used in the shield-only Step 2 OpenMC calculation properly accounts for backscattered source

particle. This section shows that the heat source and maximum concrete temperature from this approach matches the reference solution almost exactly, but the downside of this approach is that the Step 1 OpenMC eigenvalue calculation needs to model both the core and shielding region together.

- Option 2: Pursue the ES2 strategy. While this approach does not get exact agreement with the reference solution, it still retains separation of the core and shielding regions in Step 1. Depending on the particular problem, this could also be sufficiently effective in reducing the error to get better agreement with the reference R1S heat source, as was shown for the DOME shield model developed for this work. As indicated in Section 2.1.5 for a simplified geometry, this approach would likely be most optimal for low-leakage conditions in the shielding region.
- Option 3: Pursue the ES2- strategy, placing a black absorber in place of the core in Step 2 to maintain geometrical separation. This should be used with caution and verified for any specific microreactor core, as the black absorber approximation might not accurately capture the impact of a given core on particle transport inside the cavity.

2.4 Future Work

Future work for the DOME shield model includes the following modeling improvements and extensions:

- Update the DOME shield geometry with the latest design. This work was performed using the FY23 conceptual design to establish the methodology. This updated model will be uploaded to the VTB repository to be available to vendors or for confirmatory analysis purposes.
- Improve the radiative heat transfer model between the reactor and the inner shield walls. The approach presented in this report assumes infinite plate geometry for the radiative heat transfer, which results in overpredicting the concrete temperatures. Using the MOOSE ray tracing module to calculate the view factors would lead to more accurate temperature predictions and allow using more complex geometries for the reactor shape than the box that was used in this work.
- Improve the convective heat transfer in the cavity. With the shield design used in this work, natural convection in the cavity is expected. In this work, it has been accounted for by increasing the thermal conductivity of the air in the cavity. However, the sensitivity study showed that the value of this effective thermal conductivity has an impact on the maximum concrete temperature. Explicitly modeling natural convection in the cavity would improve the accuracy of the concrete temperature predictions.
- Perform transient analysis where the active cooling of the water in the tank is lost.

- Add a thermomechanical analysis of the shield structure. This would model the thermal resistance between the concrete blocks and lead to a more realistic temperature distribution.
- Use other reactor types in the cavity with various powers and leakage fractions. This will ensure the results presented in this report are valid for a wide range of reactors. This can be extended to a parameter study to determine a range of acceptable reactor designs that would meet the DOME shield limits.
- Generate dose rate maps in the DOME facility.
- Use a realistic reactor model with its primary cooling system in the thermal model to estimate the impact of the DOME shield on the reactor temperatures.
- Develop and apply variance reduction techniques to ensure high-quality heating data deep within the shield.

3. REPOSITORY UPDATES

3.1 New Models Ported in FY24

Separately from the development of the DOME models, new advanced reactor models are routinely uploaded to the [VTB repository](#). Table 6 shows a list of the models uploaded, submitted to the repository, or under export control (EC) review to the date of writing this report. More models are expected to be uploaded by the end of the FY.

Table 6. Models uploaded to the VTB repository in FY24.

Name	Reactor type	Simulation type	Sponsor	Status
Generic Pebble Bed HTGR Pronghorn tutorial	HTGR*	Thermal hydraulics	ART,NRIC	Merged
Advanced Burner Test Reactor Cross Section Generation and Full-Core Eigenvalue Calculation	SFR*	Neutronics	NEAMS	Merged
2D Ring Model for the High Temperature Test Facility	HTGR	Thermal hydraulics	NEAMS	Merged
Micro Reactor Drum Rotation model	Microreactor	Multiphysics	NEAMS	Merged
Gas-Cooled Microreactor Core	Microreactor	Neutronics	NEAMS	Merged
Effect of Partial Blockages in Simulated LMFBF Fuel Assemblies	SFR	Thermal hydraulics	NEAMS	Merged
HPMR H2 Direwolf Steady State Model	Microreactor	Multiphysics	INL-LDRD	Merged
Lotus Griffin-Pronghorn Steady State Model	MSR*	Multiphysics	NEAMS	Merged
Heat-Pipe Microreactor Assembly	Microreactor	Multiphysics	NEAMS	Merged
MSR seismic analysis	MSR	Seismic analysis	DOE-OTT*	Merged
Generic FHR Multiphysics core model	FHR*	Multiphysics	NRC*	Merged
Kilopower Reactor Using Stirling Technology (KRUSTY)	Microreactor	Multiphysics	NEAMS	Merged
Cardinal 7-pin LFR demonstration	LFR*	Multiphysics	NEAMS	Submitted
Aerojet General Nucleonics 201 Research Reactor	Research reactor	Mesh	NNSA	Under EC review
MHTGR core model	HTGR	Mesh	NEAMS	Under EC review
Generic heat-pipe Microreactor	Microreactor	Mesh	NEAMS	Under EC review

Pebble Bed Modular Reactor	HTGR	Mesh	NRC	Under EC review
SAM-Griffin Model of HTR-PM	HTGR	Multiphysics	NRC	Under EC review

* High-temperature gas reactor (HTGR); sodium fast reactor (SFR); molten-salt reactor (MSR); DOE Office of Technological Transitions (DOE-OTT); fluoride-salt-cooled high-temperature reactor (FHR); Lead Fast Reactor (LFR); Nuclear Regulatory Commission (NRC)

3.2 Workflow improvements

3.2.1 Creation of Templates for Contributions on GitHub

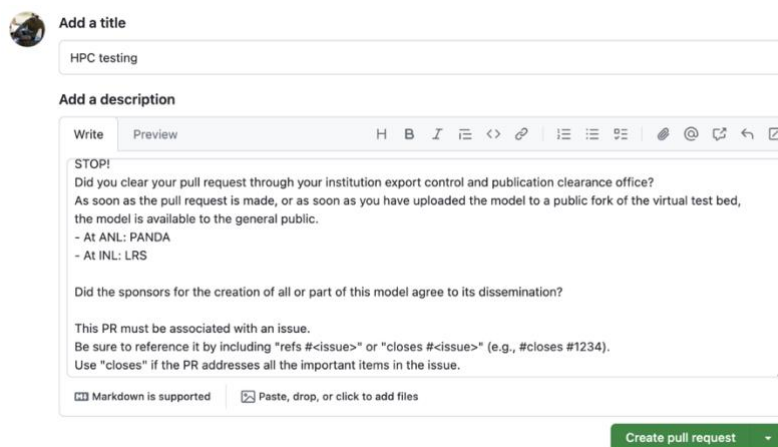
The VTB involves both new and repeat contributors every year. Repeat contributors often contribute models for their institution even though they were not the main author of the models. To streamline the process for both types of contributors, a contribution workflow was created in a “How to contribute” page. This page explains how the submissions should be formatted, what they should contain, and how to submit them. This year, we expanded the workflow by introducing GitHub pull requests and issue templates. These guide the contributors in their interaction with the repository.

Pull requests and issue templates have been deployed on the VTB GitHub repository. In the VTB repository, issues can be used to report bugs (either in the test bed or in the models), to request new models or model features, and to request test bed features. They are also used as announcements before contributing a new model. All these operations now follow an issue template, where the user or developer simply fills out the expected items for each type of interaction.

Pull requests are used to contribute models or to modify the repository and documentation. GitHub templates enable a preformatting of this user-generated content. This helps users and developers provide sufficient content on issues and pull requests. Figure 3-1 shows the beginning of the pull request template, which reminds contributors of the rules to be followed when contributing.

3.2.2 High-Performance Computing Integration

Additional integration of the VTB with high-performance computing architecture is scheduled for the end of the FY. A number of computationally-expensive reactor simulation models will leverage high-performance computing for continuous integration purposes. The infrastructure needed to implement the automated test of these models has been deployed. It has been made available very recently to the VTB team and will be integrated with VTB testing.



The screenshot shows a web form for creating a pull request. At the top, there is a profile picture icon and the text "Add a title". Below this is a text input field containing "HPC testing". Underneath is a section titled "Add a description". This section contains a rich text editor with a "Write" tab selected. The editor has a toolbar with icons for bold, italic, link, and other formatting options. The text inside the editor reads: "STOP! Did you clear your pull request through your institution export control and publication clearance office? As soon as the pull request is made, or as soon as you have uploaded the model to a public fork of the virtual test bed, the model is available to the general public. - At ANL: PANDA - At INL: LRS Did the sponsors for the creation of all or part of this model agree to its dissemination? This PR must be associated with an issue. Be sure to reference it by including "refs #<issue>" or "closes #<issue>" (e.g., #closes #1234). Use "closes" if the PR addresses all the important items in the issue." Below the editor, there are two checkboxes: "Markdown is supported" and "Paste, drop, or click to add files". At the bottom right, there is a green button labeled "Create pull request".

Figure 3-1. Pull request template, reminding the potential contributor that an EC step must be performed before contributing.

3.2.3 Trainings and Workshop Sessions

VTB is leveraged to deliver tutorials for various capabilities of the NEAMS tools for advanced reactor modeling. For example, at the 2024 American Nuclear Society summer conference, a tutorial for group cross section generation for sodium fast reactors (SFR) was given by a team from Argonne National Laboratory. The tutorial was hosted on the VTB, which displayed tutorial content that could be downloaded by trainees with access to Griffin. The VTB is additionally used for training stakeholders on NEAMS-based tools including the Nuclear Regulatory Commission and universities.

3.3 Website Improvements

With close to 50 models published on the VTB, it became both more difficult to find models without a clear idea of what they reactor they pertained to, and more advantageous to group models that feature certain characteristics together. For this purpose, a custom-made search engine on the VTB website was developed in FY23 and has been improved in FY 24. The search engine relies on contributors tagging their models with each of their characteristics. Models were already manually grouped by reactor, application, and simulation types. We can now also sort by geometry modeled, transient type, computing need, simulation features, contribution year, contributing entity, and development sponsor. New filters can be easily added in the documentation of each model. The simulation features filter is particularly helpful to find examples of novel features in the NEAMS tools deployed on models in the VTB.

This search engine uses a JavaScript back-end that runs on the visitor's browser, as the website is static for simplicity and cybersecurity reasons. As shown in Figure 3-2, users make their selections in the filters on the left of the screen. If two filters within the same category are selected, the union of the sets of results is shown. Additional filters within other categories narrow down the results with an intersection. For example, selecting the molten-salt reactor (MSR) and the high-temperature gas reactor (HTGR)

reactor types will yield all MSR and HTGR models. But selecting control rod transients for the simulation type will restrict all these models to the control rod transient type. In the left figure, we show that selecting the HTGR reactor types greys out several model “geometry” categories, because there are no models on the VTB that feature both an HTGR and those geometries. On the right, the figure shows the integration of media files and abstracts in the search engine results. These upgrades are still under development and will be deployed on the VTB by the end of the FY. This improves usability, as the additional information helps users decide which model to visit directly from that page.

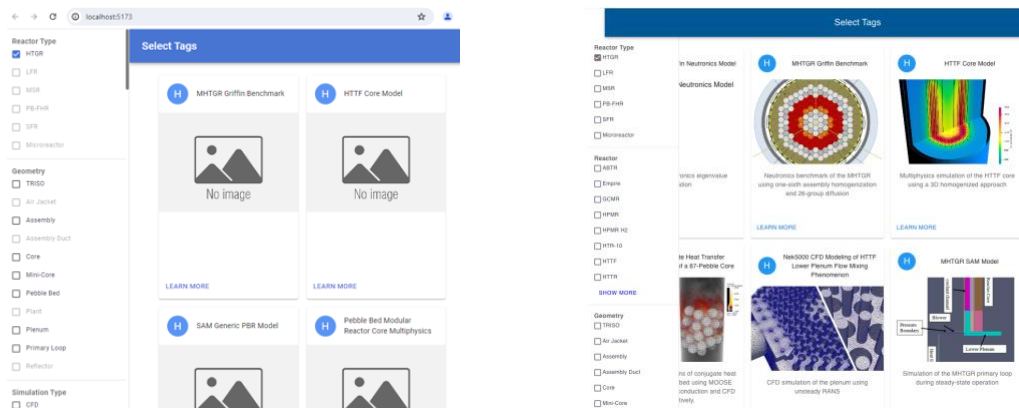


Figure 3-2. Screenshots from the additional developments of the filtering capability.

Another feature developed this FY is the automated generator of the database generation from search engine database. The sorted data information can now be output to CSV, which can then be examined using Microsoft Excel. This helps the VTB team keep track of contributions each FY and was used to generate Table 6.

3.4 Repository Maintenance

The VTB requires continuous maintenance, notably to keep the models operational and improve their documentation. Table 7 summarizes the maintenance operation performed on the VTB over the last FY. Each maintenance operation may have affected multiple models and their documentation, so counting the number of operations does not give a comprehensive picture. New model and new tutorial contributions as well as repository infrastructure changes are included as well.

Table 7. Repository maintenance in FY24.

Operation	FY23	FY24
Repository maintenance	2	-
Model maintenance	2	4
Model documentation	13	3
Repository new infrastructure	6	1 (search engine related)
New model contribution	17	11 (+5 in progress)
New tutorial contribution		1 (PBR, early October 23)

4. CONCLUSION

The VTB in FY24 had another significant year of growth.

The VTB team started modeling the NRIC DOME test bed in a shared effort between INL and Argonne National Laboratory. An initial model has been developed to evaluate the temperature distribution in the concrete shield during steady state operation, including neutron and gamma heating effects. Various modeling strategies have been examined to understand their applicability and limitations with different reactor designs to ensure the workflow is as reactor-agnostic and computationally effective as possible to maximize its usability.

The number of models hosted steadily increased, with contributions and sponsorship from an ever-greater number of institutions. The gFHR multiphysics core model for example was contributed with Nuclear Regulatory Commission sponsorship. The MSR plant seismic analysis was contributed with funding from the DOE Office of Technological Transitions. The Aerojet General Nucleonics Model mesh was funded by the DOE National Nuclear Security Administration.

The diversity of the advanced reactor landscape is further captured in the VTB, now including every major micro-reactor concept, from KRUSTY to gas cooled designs, university reactors, and benchmark reactor cases for all major reactor types.

The maintenance effort remains steady, and a balance is continuously struck between engaging resources for maintenance and other development activities.

5. REFERENCES

- [1] P. L. Schoonover, II. 2023. "SPC-70646 Specification for Reactor Supplemental Shielding for Use in DOME." Tech. Rep. INL/MIS-23-73947, Idaho National Laboratory. <https://doi.org/10.2172/1998554>.
- [2] MPR associates. 2023. "DOME Reactor Supplemental Shielding Conceptual Design." 1129-0298-RPT-001, Revision 1 B, 2023.
- [3] A. Novak, D. Andrs, P. Shriwise, J. Fang, H. Yuan, D. Shaver, E. Merzari, P. Romano, and R. Martineau. 2022. "Coupled Monte Carlo and Thermal Fluid Modeling of High Temperature Gas Reactors Using Cardinal." *Annals of Nuclear Energy*, 177, 109310. <https://doi.org/10.1016/j.anucene.2022.109310>.
- [4] P. Romano, N. Horelik, B. Herman, A. Nelson, B. Forget, and K. Smith. 2015. "OpenMC: A State-of-the-Art Monte Carlo Code for Research and Development." *Annals of Nuclear Energy*, 82, 90–97. <https://doi.org/10.1016/j.anucene.2014.07.048>.
- [5] G. Giudicelli, A. Lindsay, L. Harbour, C. Icenhour, M. Li, J. E. Hansel, P. German, P. Behne, O. Marin, R. H. Stogner, J. M. Miller, D. Schwen, Y. Wang, L. Munday, S. Schunert, B. W. Spencer, D. Yushu, A. Recuero, Z. M. Prince, M. Nezdyur, T. Hu, Y. Miao, Y. S. Jung, C. Matthews, A. Novak, B. Langley, T. Truster, N. Nobre, B. Alger, D. Andrš, F. Kong, R. Carlsen, A. E. Slaughter, J. W. Peterson, D. Gaston, and C. Permann. 2024. "3.0 - MOOSE: Enabling Massively Parallel Multiphysics Simulations," *SoftwareX*, 26, 101690. <https://doi.org/10.1016/j.softx.2024.101690>.
- [6] P. A. Behne, M. K. Jaradat, N. Choi, S. Terlizzi, and V. M. Laboure. 2023. "Development of a Bluecrab/MELCOR Framework for Supporting Realistic Mechanistic Ssource Term Calculations in Microreactors." INL/RPT-23-74793, , Idaho National Laboratory. <https://doi.org/10.2172/2203272>.
- [7] J. Dorville, G. Ridley and P. Romano. n.d. "Pull Request 2888: Storing Surface Source Points using a Cell ID." <https://github.com/openmc-dev/openmc/pull/2888>.
- [8] P. Romano, P. Shriwise, S. Harper, A. Nelson, J. Shimwell, A. Johnson, J. Tramm, Olek, J. Liang, A. Lund, G. Ridley, E. B. Knudsen, E. Peterson, R. Delaporte-Mathurin, G. Giudicelli, Y. Park, sam, A. Davis, M. Kreher, I. Meyer, A. Novak, O. Schumann, K. Kiesling, Jiankai, P. Myers, N. Horelik, L. Gross, Z. Han, dryuri92, and J. May. 2024. "openmc-dev/openmc: OpenMC 0.15.0." <https://zenodo.org/records/12215755>
- [9] D. Brown, M. Chadwick, R. Capote et al. 2018. "ENDF/B-VIII.0: The 8th Major Release Of The Nuclear Reaction Data Library with CIELO-Project Cross Sections, New Standards and Thermal Scattering Data." Nuclear Data Sheets, 148, 1–142, <https://doi.org/10.1016/j.nds.2018.02.001>.

Appendix A

Discussion on ES1 Approach Limitations

Appendix A

Discussion on ES1 Approach Limitations

In the case of a particle re-entering in the shield multiple times, the Enhanced Step 1 (ES1) approach is not strictly equivalent to the reference approach. The following figure represents the trajectory of a particle emitted from point O that scattered back from Point S and was captured at Point C.

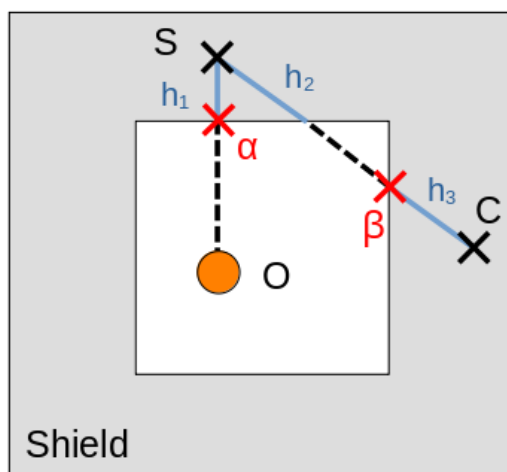


Figure A-1. Trajectory of a particle entering a shield twice.

During its travel, the particle entered the shield (represented in gray) two times at locations α and β (represented in red). The symbols h_1 , h_2 , and h_3 represent the energy deposited by the particle for the three sections of its travel inside the shield (represented in blue solid lines). If we consider a simulation running only two particles with this trajectory being the only outcome possible, the R1S approach will tally the contribution of this trajectory two times:

$$H_{R1S} = \frac{(h_1 + h_2 + h_3) + (h_1 + h_2 + h_3)}{2} = h_1 + h_2 + h_3,$$

where H_{R1S} is the heat deposited in the shield estimated with the R1S approach. If we consider two particles with the same trajectory as the one presented in the first step of the ES1 approach, four entries will be stored in the surface source bank corresponding to each time the particle entered the shield (two times: one at location α and one at location β) multiplied by the number of particles simulated (two with identical trajectory). As a result, the surface current tally T_1 defined at the inner surface of the shield will give two particles crossing per particle simulated. If we only use two particles in the fixed source calculation, the heat deposited in the shield estimated with the ES1 approach and normalized using the current T_1 can be calculated with:

$$H_{ES1} = T_1 \left(\frac{H_a + H_b}{2} \right) = 2 \left(\frac{H_a + H_b}{2} \right) = H_a + H_b,$$

where H_a and H_b are the heat contributions of two randomly selected particles a and b from the surface source bank populated in Step 1. Assuming that particles in Step 2 follow the trajectory shown in Figure A-1, the two particles stored in the surface source bank that are located at location α will scatter back at point S and then be stopped when leaving the shield because the inner surface of the shield is a vacuum boundary condition in Step 2 of the ES1 approach. Similarly, the two particles located at location β will only travel to point C to be captured. Depending on which particle is randomly selected from the source bank, three different outcomes are possible to tally the heat H_{ES1} deposited in the shield as summarized in Table 8. The heating results obtained with the ES1 approach can therefore differ from what is obtained with the R1S approach, but they should tend to be relatively close with an infinite number of simulated particles.

Table 8. Heat H_{ES1} deposited in the shield for different outcomes using the ES1 approach

Birth location of particle a	Birth location of particle b	H_{ES1}
α	β	$h_1 + h_2 + h_3$
α	α	$2(h_1 + h_2)$
β	β	$2h_3$